Nanophotonic biosensors using hexagonal nanoring resonators: computational study

Fu-Li Hsiao
National University of Singapore
Department of Electrical and Computer Engineering
4 Engineering Drive 3
Singapore, Singapore 117576
and
National Changhua University of Education
Graduate Institute of Photonics
No. 1, Jin-De Road
Changhua City, 500, Taiwan

Chengkuo Lee
National University of Singapore
Department of Electrical and Computer Engineering
4 Engineering Drive 3
Singapore, Singapore 117576
E-mail: elelc@nus.edu.sg

Abstract. The characteristics of biochemical sensors based on photonic crystal (PC) resonators are investigated in this work. The PC structure consists of holes arranged in a hexagonal lattice on a silicon slab. The nanoring resonator is formed by removing certain holes along a hexagonal trace. The hexagonal nanoring resonator is sandwiched by two PC waveguides that are formed by removing two lines of holes. The trapping of biomolecules, e.g., DNAs or proteins, in a functionalized sensing hole introduces a shift in resonant wavelength peak in the output terminal. We demonstrate two resonator designs: single and dual nanorings. The quality factor of the single nanoring resonator is 2400. The dual nanoring resonator reveals two different resonant modes. The propagated directions of dropped light for these two modes are antiparallel. The quality factors for these two resonant modes are 2100 and 1855, respectively. This dual nanoring resonator has a novel sensing mechanism, making it capable of simultaneously sensing two different biomolecules. [DOI: 10.1117/1.3532834]

Subject terms: photonic crystals; sensor; biosensor; resonator; nanoring.

Paper 09192SSRR received Dec. 31, 2009; revised manuscript received Nov. 3, 2010; accepted for publication Nov. 16, 2010; published online Feb. 28, 2011.

1 Introduction

Micro-optical and nanophotonic sensing mechanisms for chemical and biochemical sensing applications have recently attracted considerable attention. For instance, integrated optical directional couplers[1] and photonic-crystal-based Bragg gratings[2] have already been adopted for chemical and biochemical sensing. Optical sensing is typically achieved by two mechanisms. The first mechanism relies on the detection of a change in refractive index of the homogeneous medium surrounding the sensing element in the optical sensors. The second sensing mechanism is surface sensing. The optical output characteristics are the function of the thickness of biomolecules immobilized on the surface of the optical sensors.[3–5] The label-free affinity-based optical biosensors allow us to study the selective binding between the target molecules and captured agents without using a fluorescence or radio label. Surface plasma resonance and colorimetric resonance in a diffractive grating surface have also been extensively employed in commercial label-free affinity-based optical biosensors. These sensors enable the detection of selective binding of biomolecules by measuring the change of refractive index on the surface. However, the sensing area of these sensors are usually in mm^2 scale and not convenient for trace sensing.

Waveguide-based microring resonator have also received much attention in sensing applications.[6–8] The sensing area is relatively smaller than those devices based on surface plasma resonance and diffractive grating. The microring resonator configuration consists of a ring waveguide sandwiched by two straight waveguides. These two waveguides are commonly referred to as bus and drop waveguides, respectively. The whispering-gallery resonant mode of ring waveguides is excited by a broadband light source, which is carried by the bus waveguide. The resonant energy within the ring waveguide is further coupled to the drop waveguide. The resonant condition of microring resonators is extremely sensitive to the change in refractive index of the ambient medium. De Vos et al. have reported a protein concentration sensor based on a microring resonator packaged inside a microfluidic channel.[9] The sensitivity of this sensor is 10 ng/ml, with a footprint of 10×10 μm^2. The sensitivity of the microring resonator depends on the bandwidth of the resonant peak. A narrowband width reveals finer distinguishable wavelength shift, hence the sensitivity is enhanced. In addition, the bandwidth of the resonant peak decreases with an increase in the quality factor. To enhance the quality factor of the microring resonator, the reduction of ring radius is required. However, this will result in obvious increment of bending loss in the microring resonator.[5]

Compared to traditional dielectric waveguide sensing devices, nanophotonic sensors, e.g., silicon photonic crystal (PC) sensors, provide a higher potential platform. Photonic crystals consist of periodic arrays of scatters in certain matrices. This periodic spatial variation of refractive index generates the photonic bandgap (PBG) effect. Any wavelength of light that falls within the PBG range will be forbidden to propagate inside the PC structure.[10,11] By introducing certain defects within the periodic structure of the PC, light within the PBG range can be manipulated. Light is only allowed to propagate along the defects or is localized within the defects. Due to ultraefficient light confinement, PC structures can be adopted for use as optical waveguides or optical resonators of high efficiency.[12] It has been reported that a PC laser can be achieved by PC waveguide ring resonators.[13,14] In terms of sensing applications, the localized mode of electromagnetic

1932-5150/2011/$25.00 © 2011 SPIE

waves is sensitive to the variation in the refractive index of the scatters. For example, the scatters in 2-D silicon-based PC structures can be formed by drilling periodic arrays of holes on a silicon slab. When the PC structure is immersed in solutions of varying concentrations, the PBG wavelength range will change accordingly. Buswell et al. demonstrated the sensing of proteins by measuring the shift in cut-off wavelengths of a PC waveguide. They adopted the immobilized biotin as a probe to capture a 2.5-nm-thick streptavidin film on the whole PC waveguide surface. The cut-off wavelength showed a red-shift of 0.86 nm.[15] On the other hand, the resonance of a PC resonator reveals a high quality factor due to the high efficiency confinement of light. As previously mentioned, the higher quality factor represents a narrower bandwidth of resonant peak, i.e., a higher sensing resolution. Chow et al. illustrated the detection of ambient-induced refractive index change by measuring the resonant wavelength shift of 2-D PC microcavity resonator.[16] It has also been reported that a 2-D PC microcavity resonator of similar design is able to detect a mass of protein as small as 2.5 fg,[17] a gold nanoparticle 10 nm in diameter,[18] and ion concentration absorbed in an ion-selective polymer coated on the resonator.[19] In addition to the 2-D PC structure, a 1-D PC structure, which consists of one row of holes on a silicon waveguide, exhibits PBG effects as well. A 1-D PC nanocavity resonator can be formed by removing several holes.[20] Such 1-D PC nanocavity resonators have already been adopted for biosensing[21] and fluidic sensing.[22]

The sensing area of biosensors based on PC resonators is much smaller than that of a dielectric waveguide ring resonator. The resonant volume of a PC resonator is small, which makes it sensitive to the slightest change in ambient refractive index. Furthermore, this PC resonator reveals high quality factors, making it suitable for sensing extremely small volumes of analytes. The immobilization of protein and DNA in nanometer scale patterns can be achieved by direct-write dip-pen nanolithography (DPN).[23,24] The DPN technology enables us to immobilize the analyte on a single or specific holes within PC resonators. As a result, it is technically feasible to detect specific biomolecules of extremely small volume, e.g., 1 fL, captured within a small hole. Recently, the authors theoretically demonstrated a PC biosensor[25] with a footprint size of 3 μm^2. In this work, we have theoretically demonstrated the feasibility of utilizing PC nanoring resonators and PC waveguides for biochemical sensing applications. The PC structure consists of holes arranged in a hexagonal lattice on a silicon slab. The nanoring resonator is formed by removing certain holes along a hexagonal trace. The hexagonal nanoring resonator is sandwiched by two PC waveguides, which are formed by removing two lines of holes. We investigated two types of configurations: a single nanoring resonator and a dual nanoring resonator. The sensitivity with respect to the position of sensing holes within the nanoring resonantor is examined in detail.

2 Single Nanoring Resonator Sensor

The 2-D PC resonators, consisting of cascaded cavities of point defects[26] and square ring defects,[27,28] have been extensively studied. Owning to its outstanding optical confinement, the footprint of the ring defect can be significantly downsized without the risk of increase in bending loss. In

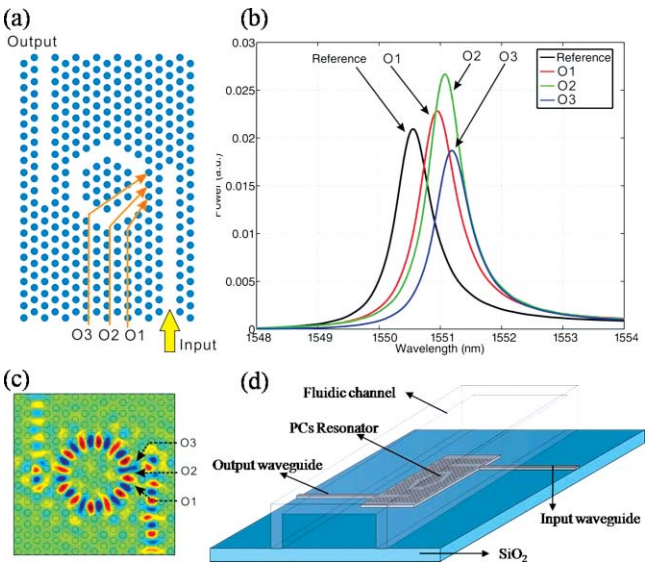

Fig. 1 (a) Sketch of nanoring resonator. (b) Spectra of reference and sensing holes at O1, O2, and O3. (c) Steady resonant field distribution. (d) Conceptual drawing of a microfluidic chip with a nanoring resonator embedded inside the microfluidic channel. (Color online only.)

our study, we created a hexagonal defect within the PC structure as a nanoring resonator. The nanoring resonator is illustrated in Fig. 1(a). Compared to the nanoring resonators in a square lattice, the bending angle of the hexagonal nanoring resonator is not as sharp as the square ring resonator. As such, the effect of the counterpropagating mode[29] can be significantly suppressed. Furthermore, the filling factor of the hexagonal lattice PC structure is higher than the square lattice PC structure, leading to superior light confinement and wider bandgap range. The quality factor can therefore be enhanced. In Fig. 1(a), the 2-D PC nanoring resonator can be considered to be fabricated on a silicon-on-insulator (SOI) wafer. The thickness of the device layer is 220 nm. DPN technology is used to perform the surface process on certain holes, e.g., deposition of probe molecules within the hole. This hole is termed the sensing hole. After the DPN process, the device is embedded in a microfluidic channel, as shown in Fig. 1(d). The entire surface of the PC structure is considered to be covered by water in our studies.

Both the effective refractive index (ERI) and 2-D finite-difference time-domain (FDTD) method are employed to simulate the performance of a resonator and derive the resonant spectra. The ERI approach and 2-D FDTD method have been widely deployed in PC slab studies.[30–34] The lattice constant (a) of the hexagonal lattice is 410 nm and the radius of holes (r) is 120 nm. The ERIs of silicon and water are 2.825 and 1.33, respectively. We adopted commercial software to perform the FDTD simulation. In the FDTD simulated model, one lattice constant is divided into 25 spatial grids. To calculate the PBG range, a transverse electric (TE) polarized light pulse, i.e., the electric field is parallel to the surface of the silicon device layer, is launched into the perfect PC structure, i.e., without any defect. The central wavelength of input light pulse is located at 1550 nm. One temporal period of the central wavelength is divided into 128 steps in the FDTD simulation. The temporal transmitted

signal is recorded by a time monitor. The transmitted spectrum is obtained by performing the fast-Fourier-transform (FFT) methods on the temporal signal. The corresponding wavelength range of PBG extended from 1423 to 1640 nm. The bandgap range is in agreement with the band structure calculated by 3-D plane wave expansion methods.

In Fig. 1(a), the PC nanoring resonator is sandwiched by two terminal PC waveguides that are formed by removing two rows of holes. The terminal waveguide at the right side of the nanoring resonator is designated as the bus waveguide. The resonant mode of the nanoring resonator is excited by the light from the input end of the waveguide (marked by the yellow arrow). The resonant light then couples to the terminal waveguide on the left side, i.e., the drop waveguide. The dropped light can be detected at the output end. In the simulation model, a temporal light pulse is launched into the bus waveguide. The output signal is recorded by a time monitor placed at the output port of the drop waveguide. The output spectrum is obtained by applying the FFT to the temporal signal. The spectrum is then normalized to the input signal. The black curve in Fig. 1(b) represents the reference output spectrum. The output resonant wavelength is 1550.5 nm. The derived quality factor is 2400. As previously mentioned, DPN technology is capable of depositing the probe molecules, e.g., antigen to antibody and DNA probe to DNA, within certain sensing holes. When the target biomolecules are carried by the fluidic flow and transited through the sensing hole, they are trapped within the sensing hole. Therefore, the ERI within the sensing hole is turned into that of the biomolecules. In our simulation, we assumed that the ERI of biomolecules is 1.45.[17,35,36] We have also chosen various hole positions as sensing holes. The positions of the sensing holes under investigation are denoted as O1, O2, and O3, respectively, in Fig. 1(a). The corresponding output spectrum of O1, O2, and O3 are represented in Fig. 1(b) by red, green, and blue lines, respectively. The curves of O1, O2, and O3 show a red shift of 0.4, 0.55, and 0.65 nm, respectively. The results reveal that the resonant intensity and quality factor are affected by the positions of the sensing holes as well.

Further calculation on the steady resonant field distribution of the nanoring resonator was done to clarify the relationship between the positions of the sensing holes and resonant wavelength shift. To obtain the steady resonant field distribution, the temporal pulse light source is replaced by a monofrequency continuous light source in FDTD simulation. The wavelength of the monofrequency light source is set to be the same with the resonant wavelength, i.e., 1550.5 nm. The steady out-of-plane magnetic field is represented by a color map in Fig. 1(c). The fields in the red and blue zones are out of phase. The darkness of the red or blue zone denotes the relevant intensity of the localized magnetic amplitude, i.e., a darker color represents a larger amplitude. The positions of O1, O2, and O3 are denoted by arrows. The magnetic field strongly penetrated through the silicon matrix among O1, O2, and O3. As such, the alteration of ERI within these sensing holes leads to significant resonant wavelength shift.

3 Dual Nanoring Resonator Sensor

3.1 *Multiple-Sensing Mechanism*

The propagated direction of dropped light in PC resonators is strongly related to the symmetry of steady resonant field distribution.[26–28] The cascading of PC resonators can be adopted to control the propagated direction of dropped light. On the other hand, cascading of cavities leads to the enlargement of resonant field distribution volume, i.e., more resonant modes. Each resonant mode corresponds to an independent resonant field distribution. In this section, we demonstrated a dual nanoring resonator with two individual resonant modes, capable of multiple sensing mechanisms.

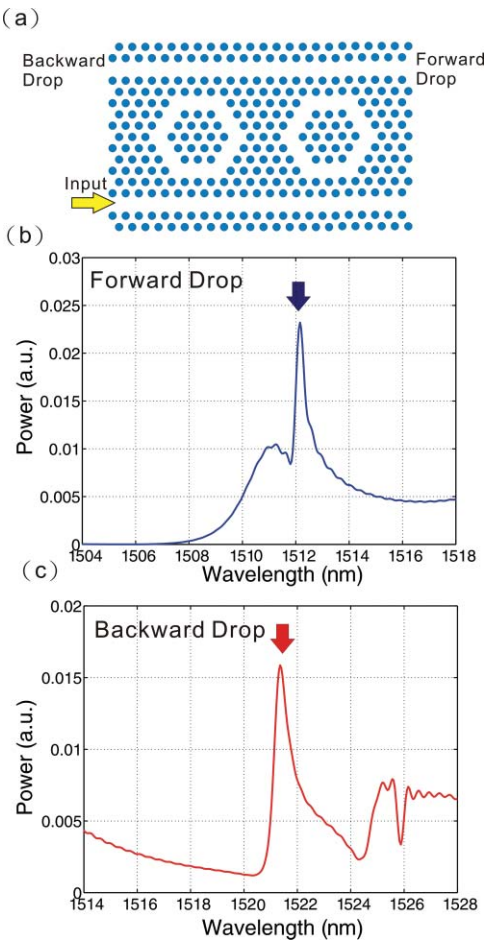

Fig. 2 (a) Sketch of dual nanoring resonator. (b) Spectra of forward drop and (c) backward drop.

Figure 2(a) illustrates the configuration of the dual nanoring resonator. The lattice constant of the PC structure is kept the same as the single nanoring PC resonator, i.e., 410 nm. The radius of holes, however, is modified to 145 nm. The two nanorings are sandwiched by two PC waveguides. The input light is launched into the input (marked by a yellow arrow) of a bus waveguide located under the dual nanoring resonator. The resonant modes of the dual nanoring resonator are excited by input light and coupled into the drop waveguide, which is located above the dual nanoring resonator. The drop waveguide has two outputs. A forward and backward drop are defined when the propagated dropped light is parallel and antiparallel to the input light, respectively. There are three holes in-between the nearest vertexes of these two nanorings. The distance between the two nanorings and the radius of holes is optimized to obtain two resonant modes of high quality factor and different drop directions. It is worth noticing that the resonant wavelengths and modes are signifi-

cantly dependent on the distance between two nanorings. The effect of the distance between nanorings to resonance is not linear because there are several mechanisms of interaction between the two resonators. Each mechanism corresponds to a unique resonant wavelength, quality factor, and dropped direction. Slight alteration of the distance between nanorings can lead to a significant change of resonance condition. Optimization is achieved by varying the number of holes between resonators, which creates two resonances of high quality factors and opposite dropped directions, i.e., forward and backward drop. The output spectra of forward and backward drop are shown in Figs. 2(b) and 2(c), respectively. The resonant peak wavelength of forward drop is 1512.16 nm with a quality factor of 2100. The resonant peak wavelength of backward drop is 1521.35 nm, with a quality factor of 1855. The steady resonant field distributions of forward and backward drop are shown in Figs. 3(a) and 3(b), respectively. The discrepancy between these two field distributions is significant. For the forward drop, as shown in Fig. 3(a), the magnetic field concentrates in regions within the two nanorings and the junction between the nanorings and waveguides. However, the magnetic field is very weak in the area between the two nearest vertexes of the two nanorings. For the backward drop phenomenon, the magnetic field concentrates within both nanorings and the area between the two nearest vertexes of them. However, the intensity in the junction between the nanorings and waveguides is relatively weak. According to the same scenario, we discussed in the section on single nanoring resonators, the target biomolecules can also be trapped within a sensing hole by adopting DPN technology. Due to the discrepancy between Figs. 3(a) and 3(b), we expect that the trapping of biomolecules in the sensing holes between the two nearest vertexes of the two nanorings, e.g., the holes marked by type 1 in Fig. 3(c), will only lead to a wavelength shift in the backward drop. On the other hand, the trapping of biomolecules in the sensing holes between the junction of nanorings and waveguides, e.g., the holes marked by type 2 in Fig. 3(c), will lead to a wavelength shift in the forward drop.

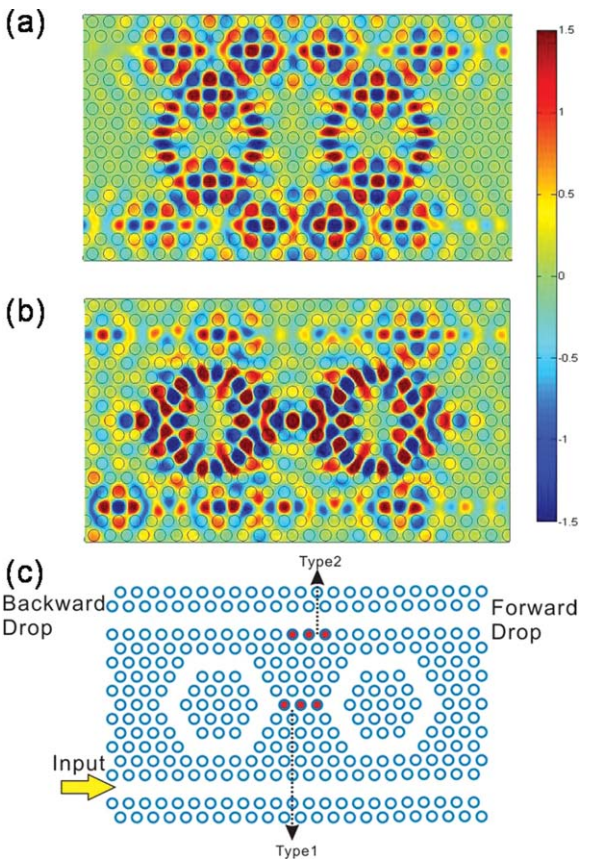

Fig. 3 Steady resonant filed distributions of (a) forward and (b) backward drop. (c) Sketch of sensing-hole position for types 1 and 2.

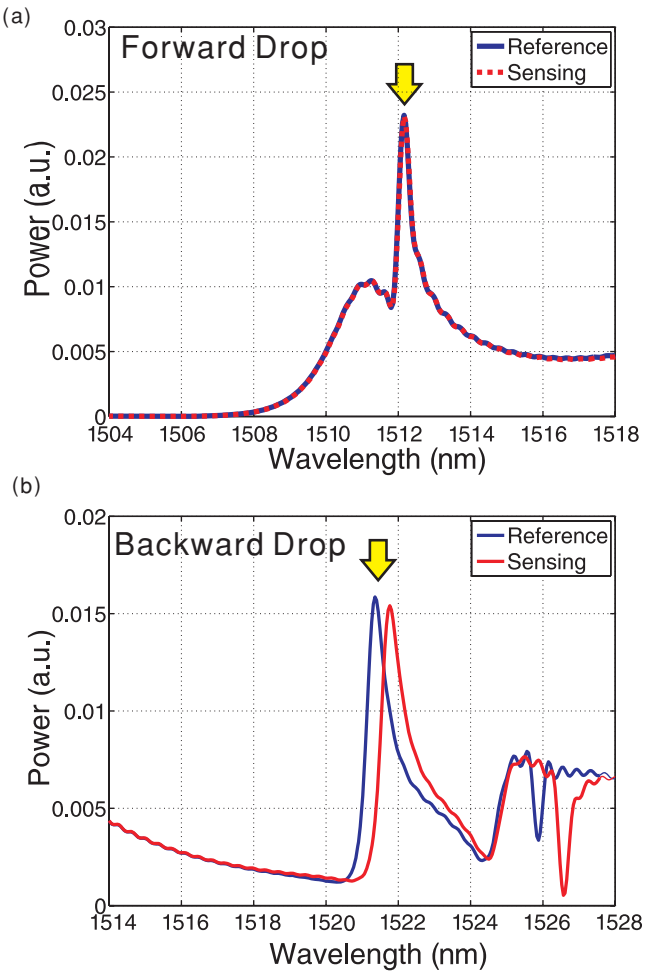

Fig. 4 (a) Forward and (b) backward drop spectra of reference and sensing cases of type 1. (Color online only.)

To verify this hypothesis, we simulated the occupation by biomolecules in types 1 and 2 sensing holes. The red dashed line in Fig. 4(a) shows the forward drop spectrum with biomolecules trapped in type-1 holes, with the reference spectrum being indicated by the blue lines. The reference spectrum represents the spectrum before the immobilization of biomolecules within the sensing holes. The blue line and red dashed line match each other. This means that the forward drop is not affected by the biomolecules. The red and blue lines in Fig. 4(b) show the backward drop spectra with biomolecules trapped in type-1 holes and reference spectra, respectively. The resonant wavelength of the red line shows a red shift of 0.41 nm. The results are in agreement with our hypothesis. To better describe quantitatively the amount

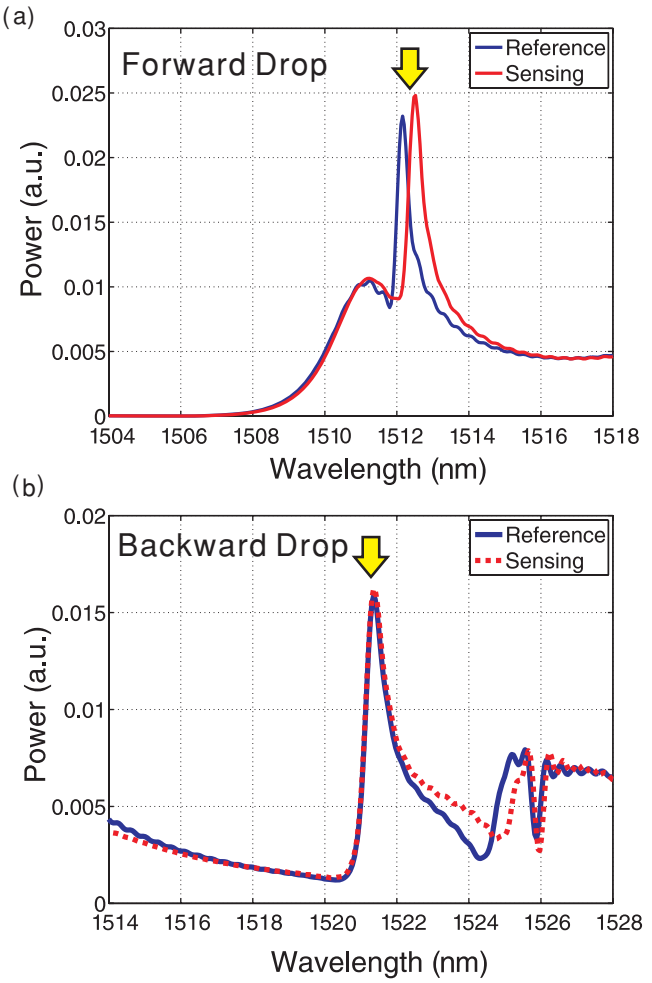

Fig. 5 (a) Forward and (b) backward drop spectra of reference and sensing cases of type 2. (Color online only.)

of biomolecules, the mass of trapped biomolecules can be evaluated by the product of volume of holes and density of biomolecules.[37] The estimated mass of the biomolecules trapped in one single hole is 1.5 fg.

Figure 5 shows the spectra of forward and backward drop, where the biomolecules are assumed to be trapped in type-2 holes. The reference spectra are also indicated by the blue lines. In Fig. 5(a), the resonant wavelength shows a red shift of 0.36 nm. The resonant wavelength of the red dashed line and blue line in Fig. 5(b) are identical. On the other hand, the resonant wavelength shift in Fig. 5(a) is smaller than the shift in Fig. 4(b). The reason is due to the intensity of the resonant magnetic field in type 2 [Fig. 3(a)] being weaker than type 1 [Fig. 3(b)].

The binding of biomolecules in sensing holes results in the change of resonant condition. The intensity, resonant wavelength, and quality factor are also altered. Such biomolecule binding may lead to the enhancement or reduction of intensity and quality factors. Unlike the single nanoring resonator, the difference in the profiles and peak intensities between the blue and red dashed lines in Figs. 4(b) and 5(a) is not significant. The reason is due to the effective resonant volume of the dual nanoring resonator being larger than the single nanoring resonator. The variation in resonant condition, with respect to the influence of ambient medium of the dual nanoring resonator, is not as sensitive as the single nanoring resonator. Furthermore, the sensing holes in the single nanoring resonator are located at the edges of the nanoring. The variation of ERI in sensing holes may affect the optical confinement, and this can lead to a significant change in resonant quality factor. As previously mentioned, sensing resolution is directly related to the quality factor. Compared to the single nanoring resonator, the intensity and quality factors of resonance in the dual nanoring resonator are more stable during the sensing process.

3.2 *Sensitivity Analysis of Single Sensing Holes*

We further investigated the resonant wavelength shift with respect to the individual position of the sensing holes. We categorized the sensing holes under study into three groups. The first group of sensing holes is denoted A1 to A10 and B1 to B10 in Fig. 6(a). These sensing holes are located along the edges of the nanorings. Figure 6(b) shows the resonant wavelength shifts with respect to the positions of sensing holes in the first group. The spectra of all sensing holes are red-shifted. The black and red symbols represent the wavelength shift of forward and backward drop, respectively. The wavelength shift of A1 to A10 equals B1 to B10. This means that the sensing effects of holes close to the bus and drop waveguides are symmetrical. The most sensitive sensing holes, i.e., the largest wavelength shifts, are A3, B3, A8, and B8. The largest wavelength shift in this group is 0.18 nm. The quality factors and intensities of the resonant peaks are

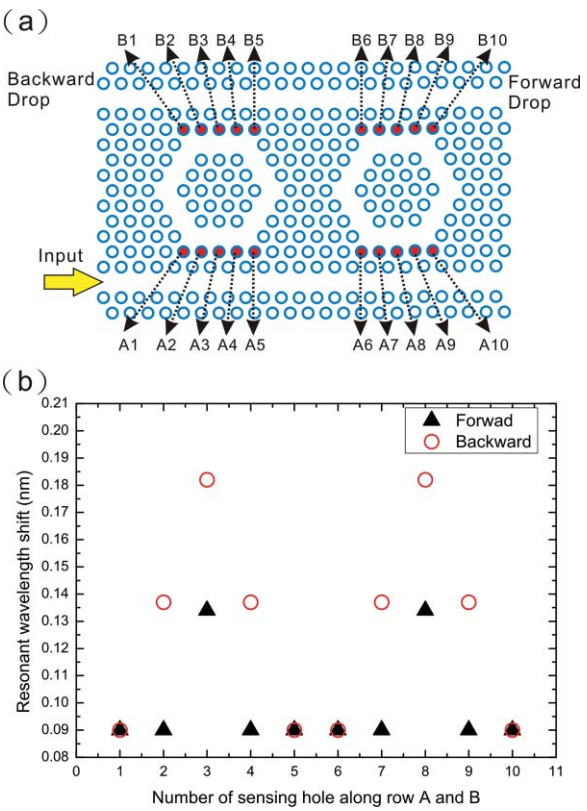

Fig. 6 (a) Sensing holes at edges of nanorings. (b) Forward and backward resonant wavelength shift in terms of position of sensing holes at A1 to A10 and B1 to B10.

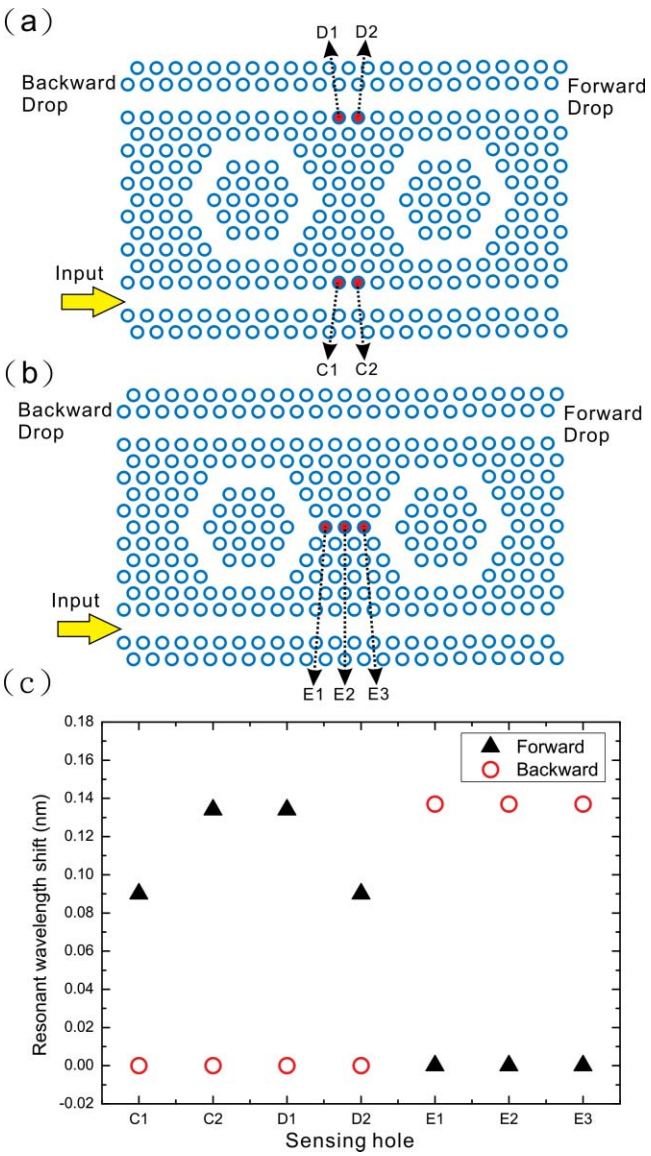

Fig. 7 (a) Sensing holes in the vicinity of waveguides in-between nanorings. (b) Sensing holes in-between the two nearest vertexes of the nanorings. (c) Forward and backward resonant wavelength shifts in terms of position of each sensing hole at (a) and (b). (Color online only.)

similar to the reference resonant peak, which we did not include in this work. Although the sensing is the same as what we chose in the single nanoring resonator, the fluctuations of resonant intensities and quality factors are not as much as in the single nanoring resonator. This result implies that the resonance in dual nanoring resonators is more stable than in the single nanoring resonator.

The second group of sensing holes is denoted by C1, C2, D1, and D2 in Fig. 7(a). These holes are located at both edges of the PC waveguide and the center of the two nanorings. Figure 7(b) shows the third group of sensing holes as E1, E2, and E3. These holes are located along the straight line between the two nearest vertexes of two nanorings. The resonant wavelength shifts of forward and backward drop are displayed by black and red symbols in Figs. 7(c), respectively. The resonant wavelength shifts show red shifts in all cases. The sensing holes of the second group only show resonant wavelength shifts in forward drop. The largest wavelength shift is 0.14 nm. There are no wavelength shifts in backward drop. On the other hand, the sensing holes in the third group show the resonant wavelength shifts in backward drop only. The largest wavelength shift is 0.14 nm. We refer to the sensing holes of the third group as backward sensing holes and those in the second group as forward sensing holes. In the previous discussion, the biomolecules are assumed to be trapped in only one single sensing hole to investigate the sensing effects of each hole. The estimated weight is as small as 1.5 fg. The wavelength shift seems quite small because only one single sensing hole is considered. In practice, we can enhance the resonant wavelength shift by choosing more than one sensing hole.

We further propose two potential applications based on features of the second and third groups of sensing holes. The first one is dual-channel detection. We can use DPN technology to assemble one kind of probe molecules on forward sensing holes and the other kinds of probe molecules on backward sensing holes. When the dual nanoring resonator is packaged inside a microfluidic channel, as depicted in Fig. 1(d), the solution carrying unknown biomolecules will flow through the dual nanoring resonator. Two kinds of target DNA molecules will be selectively trapped by the forward and backward sensing holes. The wavelength shift is proportionate to the ERI change, i.e., the amount of binding biomolecules.[38] Thus the concentration of two different target DNAs in the same solution can be detected at the same time by simultaneously monitoring the resonant wavelength shift at forward and backward drop ports. This application will be useful for studies of certain biochemical interaction processes. This also provides more versatility compared to devices that can detect only one type of molecule. The second application is real-time calibration. The resonant wavelength shift can result from not only the binding of biomolecules but also from environmental factors such as temperature change or fabrication inaccuracy. Although the response time of optical sensors is quite fast, the interaction between probe and target molecules usually takes time. It is difficult to control all of the factors contributed by the environment during the entire interaction duration. Therefore, we can trap the biomolecules in forward sensing holes and measure both the resonant wavelength shift at forward and backward drop ports. The wavelength shift of forward drop results from both biomolecule binding and factors of environment. However, the wavelength shift of backward drop results from the factors of environment only. The effects of environmental change in forward drop can hence be eliminated by the information acquired from the backward drop. In addition to dual-channel detection and real-time calibration, multichannel detection can be achieved by cascading more nanorings with various independent resonant modes, wavelengths, and drop channels.

4 Conclusions

In summary, we demonstrate the feasibility of PC single and dual nanoring resonators for biosensing applications. The PC nanoring resonator is considered to be formed by removing certain holes from a 2-D silicon PC slab. In applications of biosensing, the whole nanoring resonator is embedded inside a microfluidic channel. The sensing mechanism is based on

the red shift of resonant wavelength, owing to the trapping of analytes in particular holes. The resonant wavelength shift shows strong dependence on the position of sensing holes. PC nanoring resonators reveal high quality factors and small footprints in comparison with microring resonator. The quality factor of a single nanoring resonator is 2400. The quality factor of the forward and backward drop of a dual nanoring resonator is 2100 and 1855, respectively. The wavelength shift of a single nanoring resonator is larger than the dual nanoring resonator. However, the stability of dual nanoring resonators is better. In addition, we also explore two individual resonant modes with opposite drop directions in the dual nanoring resonator. These two resonant modes can be individually manipulated by selecting the appropriate sensing holes. We also propose that dual-channel detection and real-time calibration can be achieved by dual nanoring resonators.

Acknowledgments

The authors would like to acknowledge support from the National University of Singapore under University Research Committee Fund R-263-000-475-112, Academic Research Committee Fund MOE2009-T2-2-011, and the Agency for Science, Technology, and Research (A*STAR), SERC Grant No. 0921010049. This work is also support by Taiwan's National Science Council (NSC) under Contract No. NSC-99-2221-E-018-020.

References

1. B. J. Luff, R. D. Harris, J. S. Wilkinson, R. Wilson, and D. J. Schiffrin, "Integrated-optical directional coupler biosensor," *Opt. Lett.* **21**(8), 618–620 (1996).
2. W. C. L. Hopman, P. Pottier, D. Yudistira, J. van Lith, P. V. Lambeck, R. M. De La Rue, A. Driessen, H. J. W. M. Hoekstra, and R. M. de Ridder, "Quasi-one-dimensional photonic crystal as a compact building-block for refractometric optical sensors," *IEEE J. Sel. Top. Quantum Electron.* **11**(1), 11 (2005).
3. F. Dell'Olio and V. M. N. Passaro, "Optical sensing by optimized silicon slot waveguides," *Opt. Express* **15**(8), 4977–4993 (2007).
4. N. Skivesen, A. Têtu, M. Kristensen, J. Kjems, L. H. Frandsen, and P. I. Borel, "Photonic-crystal waveguide biosensor," *Opt. Express* **15**(6), 3169–3176 (2007).
5. X. Fan, I. M. White, H. Zhu, J. Suter, and H. Oveys, "Overview of novel integrated optical ring resonator bio/chemical sensors," *Proc. SPIE* **6452**, 64520M (2007).
6. E. Krioukov, D. J. W. Klunder, A. Driessen, J. Greve, and C. Otto, "Sensor based on an integrated optical microcavity," *Opt. Lett.* **27**(7), 512–514 (2002).
7. C. Y. Chao, W. Fung, and L. J. Guo, "Polymer microring resonators for biochemical sensing applications," *IEEE J. Sel. Top. Quantum Electron.* **12**(1), 134–142 (2006).
8. M. Kwon and W. H. Steier, "Microring-resonator-based sensor measuring both the concentration and temperature of a solution," *Opt. Express* **16**(13), 9372–9377 (2008).
9. K. De Vos, I. Bartolozzi, E. Schacht, P. Bienstman, and R. Baets, "Silicon-on-insulator microring resonator for sensitive and label-free biosensing," *Opt. Express* **15**(12), 7610–7615 (2007).
10. E. Yablonovitch, "Inhibited spontaneous emission in solid-state physics electronics," *Phys. Rev. Lett.* **58**(20), 2059–2062 (1987).
11. S. John, "Strong localization of phonics in certain disordered dielectric superlattices," *Phys. Rev. Lett.* **58**(23), 2486–2489 (1987).
12. S. Tomljenovic-Hanic, M. J. Steel, C. Martijn de Sterke, and J. Salzman, "Diamond based photonic crystal microcavities," *Opt. Express* **14**(8), 3556–3562 (2006).
13. A. R. Alija, L. J. Martínez, P. A. Postigo, C. Seassal, and P. Viktorovitch," Coupled-cavity two-dimensional photonic crystal waveguide ring laser," *Appl. Phys. Lett.* **89**, 101102 (2006).
14. S. H. Kim, H. Y. Ryu, H. G. Park, G. H. Kim, Y. S. Choi, Y. H. Lee, and J. S. Kim, "Two-dimensional photonic crystal hexagonal waveguide ring laser," *Appl. Phys. Lett.* **81**, 2499 (2002).
15. S. C. Buswell, V. A. Wright, J. M. Buriak, V. Van, and S. Evoy, "Specific detection of proteins using photonic crystal waveguides," *Opt. Express* **16**(20), 15949–15957 (2008).
16. E. Chow, A. Grot, L. W. Mirkarimi, M. Sigalas, and G. Girolami, "Ultracompact biochemical sensor built with two-dimensional photonic crystal microcavity," *Opt. Lett.* **29**(10), 1093–1095 (2004).
17. M. Lee and P. M. Fauchet, "Two-dimensional silicon photonic crystal based biosensing platform for protein detection," *Opt. Express* **15**(8), 4530–4535 (2007).
18. M. R. Lee and P. M. Fauchet, "Nanoscale microcavity sensor for single particle detection," *Opt. Lett.* **32**(22), 3284–3286 (2007).
19. S. Chakravarty, J. Topol'ancik, P. Bhattacharya, S. Chakrabarti, Y. Kang, and M. E. Meyerhoff, "Ion detection with photonic crystal microcavities," *Opt. Lett.* **30**(9), 2578–2580 (2005).
20. J. S. Foresi, P. R. Villeneuve, J. Ferrera, E. R. Thoen, G. Steinmeyer, S. Fan, J. D. Joannopoulos, L. C. Kimerling, H. I. Smith, and E. P. Ippen, "Photonic-bandgap microcavities in optical waveguides," *Nature* **390**, 143–145 (1997).
21. C. Lee, A. S. P. Yee, J. L. J. Perera, C. C. Chen, and N. Balasubramanian, "Design of nanobiophotonics resonators for biomolecules detection," *3rd Ann. IEEE Intl. Conf. Nano/Micro Eng. Molecular Syst.*, pp. 274–279 (2008).
22. S. Mandal and D. Erickson, "Nanoscale optofluidic sensor arrays," *Opt. Express* **16**(3), 1623–1631 (2008).
23. S. W. Chung, D. S. Ginger, M. W. Morales, Z. Zhang, V. Chandrasekhar, M. A. Ratner, and C. A. Mirkin, "Top-down meets bottom-up: dip-pen nanolithography and DNA-directed assembly of nanoscale electrical circuits," *Small* **1**(1), 64–69 (2005).
24. J. Haaheim, R. Eby, M. Nelson, J. Fragala, B. Rosner, H. Zhang, and G. Athas, "Dip pen nanolithography (DPN): process and instrument performance with NanoInk's NSCRIPTOR system," *Ultramicroscopy* **103**(2), 117–132 (2005).
25. F. L. Hsiao and C. Lee, "Computational study of photonic crystals nanoring resonator for biochemical sensing," *IEEE Sens. J.* **10**(7), 1185–1191 (2010).
26. S. Fan, P. R. Villeneuve, J. D. Joannopoulos, and H. A. Haus, "Channel drop filters in photonic crystals," *Opt. Express* **3**, 4–11 (1998).
27. Z. Qiang, W. Zhou, and R. A. Soref, "Optical add-drop filters based on photonic crystal ring resonators," *Opt. Express* **15**, 1823–1831 (2007).
28. F. Monifi, A. Ghaffari, M. Djavid, and M. S. Abrishamian, "Three output port channel-drop filter based on photonic crystals," *Appl. Opt.* **48**, 804–809 (2009).
29. V. Kumar, T. Srinivas, and A. Selvarajan, "Investigation of ring resonators in photonic crystal circuits," *Photonics and Nanostructures Fundamentals and Applications* **2**, 199–206 (2004).
30. M. Qiu, "Effective index method for the heterostructure-slab-waveguides-based two-dimensional photonic crystals," *Appl. Phys. Lett.* **81**, 1163 (2002).
31. S. Oliver, H. Benisty, M. Rattier, C. Weisbuch, M, Qiu, A. Karlsson, C. J. M. Smith, R. Houdre, and U. Oesterle, "Resonant and nonresonant transmission through waveguide bends in a planar photonic crystal," *Appl. Phys. Lett.* **79**, 2514–2516 (2001).
32. M. Kitamura, S. Iwamoto, and Y. Arakawa, "Enhanced light emission from an organic photonic crystal with a nanocavity," *Appl. Phys. Lett.* **87**, 151119 (2005).
33. W. Zheng, M. Xing, G. Ren, S. G. Johnson, W. Zhou, W. Chen, and L. Chen, "Integration of a photonic crystal polarization beam splitter and waveguide bend," *Opt. Express* **17**, 8657–8668 (2009).
34. Y. Chassagneux, R. Colombelli,W. Maineult, S. Barbieri, S. P. Khanna, E. H. Linfield, and A. G. Davies, "Predictable surface emission patterns in terahertz photonic-crystal quantum cascade lasers," *Opt. Express* **17**, 9492–9502 (2009).
35. H. Kurt and D. S. Citrin, "Coupled-resonator optical waveguides for biochemical sensing of nanoliter volumes of analyte in the terahertz region," *Appl. Phys. Lett.* **87**, 241119 (2005).
36. H. Ouyang, C. C. Striemer, and P. M. Fauchet, "Quantitative analysis of the sensitivity of porous silicon optical biosensors," *Appl. Phys. Lett.* **88**, 163108 (2006).
37. M. D. Bennett, J. S. Heslop-Harrison, J. B. Smith, and J. P. Ward, "DNA density in mitotic and meiotic metaphase chromosomes of plants and animals," *J. Cell Sci.* **63**(1), 173–179 (1983).
38. B. Schmidt, V. Almeida, C. Manolatou, S. Preble, and M. Lipson, "Nanocavity in a silicon waveguide for ultrasensitive nanoparticle detection," *Appl. Phys. Lett.* **85**(21), 4854–4856 (2004).

Fu-Li Hsiao received his BS degree from the Department of Physics of National Changhua University of Education, Taiwan, in 2002; and his PhD degree from FEMTO-ST of University of Franche-Comte, France, and from the Department of Optics and Photonics of National Central University, Taiwan in 2008. He has been a research fellow in the Department of Electrical and Computer Engineering at National University of Singapore from Nov. 2008 to Jul. 2009. Currently he is

an assistant professor in the Graduate Institute of Photonics at National Changhua University of Education, Taiwan. His research interests include photonic crystals, phononic crystals and optical MEMS.

Chengkuo Lee received a MS degree in materials science and engineering from National Tsing Hua University, Hsinchu, Taiwan, in 1991. He also received a MS degree in industrial and system engineering from Rutgers University, New Brunswick, NJ, in 1993. He received his PhD degree in precision engineering from the University of Tokyo, Tokyo, Japan, in Jan. 1996. He worked as foreign researcher in the Nanometer-scale Manufacturing Science Lab. at the Research Center for Advanced Science and Technology (RCAST) of the University of Tokyo from 1993 to 1996. He had also worked in Mechanical Engineering Lab., AIST, MITI of Japan as a JST research fellow in 1996. Thereafter he was a senior research staff of Microsystems Lab., Industrial Technology Research Institute (ITRI), Hsinchu, Taiwan. Since Sept. 1997, he has joined the Metrodyne Microsystem Corporation, Hsinchu, Taiwan, and established the MEMS device division and the 1st micromachining fab for commercial purpose in Taiwan. He was the manager of MEMS device division between 1997 and 2000. He had been the adjunct assistant professor in Electro-physics Department of National Chiao Tung University in 1998, and the adjunct assistant professor in Institute of Precision Eng. of National Chung Hsing University since 2001 to 2005. He co-founded the Asia Pacific Microsystems, Inc. (APM) Hsinchu, Taiwan, in Aug. 2001, and he has been the vice president (VP) of R&D at the beginning, then become the VP of optical communication business unit and special assistant of CEO in charge of international business and technical marketing for MEMS foundry service at APM, Inc. till end of 2005. From 2006 to 2009, he has been a senior member of technical staff at the Institute of Microelectronics (IME), A*Star, Singapore. He has been an assistant professor at the Department of Electrical and Computer Engineering of National University of Singapore, Singapore since Dec. 2005. He is the co-author of a book in title of *Advanced MEMS Packaging*, McGraw-Hill, 2010. He has contributed more than 130 international conference papers and extended abstracts, 80 peer-reviewed international journal articles, and 8 US patents in MEMS, nanophotonics and nanotechnology fields. He is the member of IEEE, MRS, and IEE Japan.